

The Open University's repository of research publications and other research outputs

Electron transfer driven decomposition of adenine and selected analogs as probed by experimental and theoretical methods

Journal Item

How to cite:

Cunha, T.; Mendes, M.; Ferreira da Silva, F.; Eden, S.; García, G.; Bacchus-Montabonel, M.-C. and Limão-Vieira, P. (2018). Electron transfer driven decomposition of adenine and selected analogs as probed by experimental and theoretical methods. *The Journal of Chemical Physics*, 148(13), article no. 134301.

For guidance on citations see [FAQs](#).

© [not recorded]

Version: Accepted Manuscript

Link(s) to article on publisher's website:
<http://dx.doi.org/doi:10.1063/1.5021888>

Copyright and Moral Rights for the articles on this site are retained by the individual authors and/or other copyright owners. For more information on Open Research Online's data [policy](#) on reuse of materials please consult the policies page.

Electron transfer driven decomposition of adenine and selected analogues as probed by experimental and theoretical methods

T. Cunha,¹ M. Mendes,¹ F. Ferreira da Silva,¹ S. Eden,² G. García,³

M.-C. Bacchus-Montabonel^{4,a)} and P. Limão-Vieira^{1,a)}

¹ Atomic and Molecular Collisions Laboratory, CEFITEC, Department of Physics, Universidade NOVA de Lisboa, 2829-516 Caparica, Portugal

² School of Physical Sciences, The Open University, Walton Hall, MK7 6AA, Milton Keynes, UK

³ Instituto de Física Fundamental, Consejo Superior de Investigaciones Científicas (CSIC), Serrano 113-bis, 28006 Madrid, Spain

⁴ Univ. Lyon, Université Claude Bernard Lyon 1, CNRS, Institut Lumière Matière, 69622 Villeurbanne, France

ABSTRACT

We report on a combined experimental and theoretical study of electron transfer induced decomposition of adenine and a selection of analogue molecules in collisions with potassium atoms (K). Time-of-flight negative ion mass spectra have been obtained in a wide collision energy range (6–68 eV in the centre-of-mass frame), providing a comprehensive investigation of the fragmentation patterns of purine, adenine, 9-methyl adenine, 6-dimethyl adenine and 2-D adenine. Following our recent communication about selective hydrogen loss from the transient negative ions (TNI) produced in these collisions [J. Chem. Phys. **148**, 021101 (2018)], this work focuses on the production of smaller fragment anions. In the low-energy part of the present range, several dissociation channels that are accessible in free electron attachment experiments are absent from the present mass spectra, notably NH₂ loss from adenine and 9-methyl adenine. This can be understood in terms of a relatively long transit time of the K⁺ cation in the vicinity of the TNI tending to enhance the likelihood of intramolecular electron transfer. In this case, the excess energy can be redistributed through the available degrees of freedom inhibiting fragmentation pathways. Ab initio theoretical calculations were performed for 9-methyl adenine (9-mAd) and adenine (Ad) in the presence of a potassium atom and provided a strong basis for the assignment the lowest unoccupied molecular orbitals accessed in the collision process.

^{a)} Authors to whom correspondence should be addressed. Electronic mail: plimaovieira@fct.unl.pt, bacchus@univ-lyon1.fr; P. Limão-Vieira: Tel. (+351) 21 294 78 59, M.-C. Bacchus-Montabonel: Tel. (+33) 472 43 10 83.

I. INTRODUCTION

It is now well-established within the international scientific community that *low-energy* electrons (e.g. <15 eV), as the most abundant secondary species produced by ionising radiation, play an important role in the modification of critical molecular structures in biological material. Such electron induced molecular decomposition processes have been demonstrated to yield substantial damage in plasmid DNA through single- and double-strand breaks.¹ Low-energy electrons can efficiently attach to DNA molecular constituents and derivatives to form transient negative ions (TNI), which can subsequently dissociate and have been probed extensively in recent years using both experimental and theoretical methods.² Under aqueous conditions which approximate biological environments, TNI resonances can be shifted to lower energies³. Furthermore Wang and co-workers⁴ found that significant quantities of single- and double-strand breaks of irradiated aqueous DNA are induced by pre-hydrated electrons. Wang *et al.*'s experiments on each deoxyribonucleotide (dXMP where X represents Thymine, Cytosine, Guanine or Adenine) have also shown that dGMP and dAMP are more efficient at capturing pre-hydrated electrons than dTMP and dCMP. Since most of the radiation damage in cellular DNA occurs through the generation of reactive species within the surrounding water, Wang *et al.*'s proposed mechanism of dissociative electron transfer may be responsible for a large portion of such damage. Given this rationale, electron transfer seems to be more prevalent under physiological conditions rather than free electron attachment processes. Therefore we consider that the present data on collisional electron-transfer induced dissociation of selected purine targets may have future applications in nanoscale models of radiation damage in DNA. By carrying out potassium-impact mass spectrometry experiments on partially labelled derivatives of adenine (Ad) and by means of quantum chemical calculations, we have explored the fragmentation patterns of negative ions formed in charge-transfer collisions.

Electron interactions with adenine (C₅H₅N₅) are well represented in the literature, including dissociative electron attachment (DEA) experiments,^{5,6} electron impact ionisation studies,⁷ and charge-exchange collisions with laser-excited Rydberg atoms to probe dipole-bound anions.⁸ Aflatooni *et al.*'s^{9,10} electron transmission data placed the three lowest electron affinities of π^* character at 0.54, 1.36 and 2.17 eV. More recently, site-selective bond excision of adenine yielding the dehydrogenated parent anion upon electron transfer in collision with neutral potassium atoms have been reported.¹¹ The influence of functional groups on site-specific dissociation of DNA bases by low-energy electron impact has been demonstrated via an effective loss of hydrogen located at the specific nitrogen positions.^{12,13,14} As far as theoretical investigations are concerned, we note elastic-scattering cross sections and resonance energies

for low-energy electron impact on DNA/RNA bases¹⁵, bound anionic states of adenine tautomers explored at the B3LYP/6-31+G** level of theory,¹⁶ vertical and adiabatic ionisation energies of 12 adenine tautomers,¹⁷ geometrical structures and energetic properties for different tautomers of adenine using multi-configurational wave functions,¹⁸ and electronic spectra of purines¹⁹ and purine tautomers.²⁰ Comprehensive studies on dissociative photoionisation of adenine following valence excitation²¹ and reactivity in adenine–water clusters in multi-photon and electron impact ionisation studies,²² have been also reported. Finally, hydrodynamic simulations have indicated that sequential HCN addition can be responsible for adenine formation during molecular cloud collapse.²³ Quantum chemical studies have recently shed light on the role of HCN and other prebiotic oligomers (e.g. HCCN, NH₂CN and CN) to participate in gas-phase (and in the grain-phase) radical-radical and radical-molecule reactions on adenine formation within the interstellar medium.^{24,25}

II. EXPERIMENTAL METHOD

The crossed molecular beam setup used to study collisions of neutral potassium (K) atoms with neutral purines, has been described in detail previously.^{26,27} Briefly, an effusive target molecular beam crosses a primary beam of fast neutral K atoms and the product anions are analysed using a home-built linear time-of-flight (TOF) mass spectrometer. The K beam is produced in a resonant charge exchange chamber from the interaction of K⁺ ions from a potassium ion source (12–100 eV in the lab frame) with gas-phase neutral potassium atoms from an oven source. Residual ions were removed from the primary beam by electrostatic deflecting plates outside the oven. The intensity of the neutral potassium beam was monitored using a Langmuir–Taylor ionisation detector before and after the collection of each TOF mass spectrum and the beam energy resolution in the collision energy range as measured as ~0.5 eV (FWHM) using a hemispherical electrostatic energy loss analyser to characterise the K⁺ ion signal at a fixed energy following K collisions with nitromethane. The effusive beam of purines from an oven source was admitted into vacuum through a 1 mm diameter capillary where it was crossed with the neutral fast potassium beam. Negative ions formed in the collision region were extracted by a 250 V cm⁻¹ pulsed electrostatic field. The typical base pressure in the collision chamber was 6×10⁻⁵ Pa and the working pressure was 4×10⁻⁴ Pa. Mass spectra (resolution $m/\Delta m \approx 125$) were obtained by subtracting background measurements (without the heated sample) from the sample measurements. Mass calibration was carried out on the basis of the well-known anionic species formed after potassium collisions with nitromethane.²⁸ Purine (Pu), adenine (Ad), 9-methyl adenine (9-mAd) and 6-dimethyl adenine (6-dimAd) were supplied by Sigma Aldrich with

stated purities of 98%, $\geq 99\%$, 97% and $\geq 98\%$, respectively. Adenine-2-d (2-DAd) was supplied by CDN Isotope Inc. with isotope enrichment of 97%. They were used as delivered. The samples were heated up to 400 K and the temperatures were controlled using a PID unit. In order to test for any thermal decomposition, spectra were recorded at different temperatures. No differences were observed in relative peak intensities as a function of temperature. The extraction region and the TOF system were heated during the measurements in order to prevent any sample condensation and thus charge accumulation on the electrodes.

III. THEORETICAL METHOD

The charge transfer in the collision of a neutral potassium atom and a nucleobase is described in the framework of the molecular representation looking at the evolution of the quasi-molecular system formed by the potassium projectile and the biomolecular target along the reaction coordinate. The one-dimension coordinate approximation is applied, as in previous ion/neutral-biomolecule collision systems.^{29,30,31} The atom-nucleobase collision system is thus treated as a pseudo-diatomic molecule evolving along the coordinate associated with the distance between the impinging atom and the nucleobase.^{32,33} This approach does not consider the internal degrees of freedom of the biomolecule but may be used for very fast collision processes where nuclear vibration and rotation motions are much slower than the collision time and can be frozen during the collision.

The geometry of adenine and 9-mAd has been optimized at the MP2 level of theory from the work of *Fuentes-Cabrera et al.*³⁴ A perpendicular approach of the potassium atom, pointing at the N9 atom (see FIG. 1) has been considered, as the charge transfer process has been clearly shown to be favoured in such orientation for the case of pyrimidine targets.^{35,36} Ab-initio molecular calculations have been carried out with the MOLPRO code.³⁷ The nucleobase targets are kept frozen in their ground state geometry during the collision process. The calculation has been performed in Cartesian coordinates, with no symmetries. All electrons have been considered for C, N and H atoms with the 6-311G** basis set, although the 18 core electrons of potassium have been treated through the ECP18sdf core-electron pseudopotential³⁸, with the corresponding basis set. The natural molecular orbitals for the K-Ad and K-9mAd have been determined by state-averaged CASSCF calculations for the reaction coordinate $R = 10 \text{ \AA}$ corresponding to the asymptotic region. Similar active spaces have been considered for both targets in order to compare each system at the same level of accuracy. The 1s orbitals of carbon, nitrogen and oxygen are treated as frozen cores. The resultant highest occupied molecular orbitals (HOMOs) and lowest unoccupied molecular orbitals (LUMOs) for adenine and 9-

methyl adenine are shown in FIG. 2 together with the corresponding orbitals without the presence of potassium. For adenine orbitals, the present results are in good agreement with a recent study using the CAP/SAC-CI method.³⁹ The polarization by the potassium atom induces a global shift in energy of about 2 eV for the π orbitals but the effect remains weak on the σ orbitals.

IV. RESULTS AND DISCUSSION

Our recent short communication on electron transfer from neutral potassium atoms to Pu, Ad, 9-mAd, 6-dimAd and 2-Dad showed that dehydrogenated parent anion formation can be achieved by selective breaking of C–H or N–H bonds, depending on the collision energy.¹¹ Based on the same experiments, the present work extends the analysis to the full fragmentation pattern of the TNIs. The two papers are complementary and the reader is recommended to read both for a full investigation of the collision dynamics. Dissociative electron transfer TOF mass spectra were recorded at lab-frame collision energies of 12–100 eV (3.8–68.3 eV in the centre-of-mass frame and from now on referred as available energy). TABLE I is a compilation of all fragment anions detected at 12, 15, 30, 50, 70 and 100 eV lab frame collision energies.

FIG. 3 shows the negative ion TOF mass spectra recorded at 30 eV for Pu, Ad and 6-dimAd, FIG. 4 for Ad and Pu at 70 eV, and FIG. 5 for 2-DAd and 9-mAd at 100 eV lab frame collision energies with neutral potassium atoms. Branching ratios (BRs) for the major fragments of Ad and Pu as a function of the collision energy are presented in FIG. 6. The TOF mass spectra show no evidence of parent anion formation (M^-) and are, generally speaking dominated by the cyanide anion (CN^-). The absence of M^- formation is unsurprising since the vertical electron affinity of adenine is -0.54 eV.⁹ The loss of different HCN units from the dehydrogenated parent anion of Pu and Ad, $(M-H)^-$, is schematically presented in TABLE I (see discussion in Section C). Another interesting aspect to discuss is the role of the potassium cation in the vicinity of the temporary negative ion (TNI) formed upon electron transfer, i.e. $K + M \rightarrow (K^+M^-)$ and how the strong Coulomb interaction may affect the decomposition of the TNI. This is comprehensively investigated here and a mechanism is proposed with the help of quantum chemical calculations below. From the calculations, we also note that the lowest-lying π^* states are considerably shifted to higher energies (~ 2 eV) in the presence of a potassium cation (some of the calculated MOs without the presence of K appear in parenthesis in FIG. 2).

Finally, accessing a π^* state does not lead to direct bond breaking unless a repulsive σ^* state is crossed diabatically. However, the available energy is enough to give access to intramolecular electron transfer ($\pi \rightarrow \sigma$), which is possible if the nuclear wavepacket survives long enough

along the reaction coordinate to allow diabatic coupling between the two states. This is discussed below within the scope of the different π^* and σ^* MOs involved in the formation of particular fragment anions.

A. (M-H)⁻, (M-2H)⁻ and (M-3H)⁻

The dehydrogenated closed shell anion (M-H)⁻ is observed for all the molecular targets studied here and is formed via the ion-pair reaction:



Reaction (1) represents a direct cleavage of the (C-H) and/or (N-H) bonds (the specific H removal can be selected using the collision energy as reported in Ref. 11) and (M)^{#-} means a TNI formed with an excess of internal energy. Formation of the parent ion with H abstraction has been reported in DEA experiments on adenine through vibrational Feshbach resonances¹⁴ and a weak “0 eV” contribution, the latter attributed to vibrationally excited molecules.⁶ Adenine BRs as a function of the available energy (FIG. 6a)), show that (Ad-H)⁻ is the most abundant fragment anion in the low energy collision region and its threshold of formation is below 4.0 eV (12 eV in the lab frame). This is consistent with DEA resonances at 1.07 and 1.4 eV (1.36 eV⁹) attributed to N9-H excision and 2.2 eV (2.17 eV⁹) to C6N-H bond breaking.¹⁴ Another interesting aspect of the adenine BRs is that the (Ad-H)⁻ yield is generally speaking $\geq 50\%$ below 16 eV and strongly dominates at 6.1 eV. Above this energy, the (Ad-H)⁻ BR decreases while the (CN)⁻ BR increases, becoming dominant above 30 eV. This indicates that the dehydrogenated parent anion is a precursor in the formation of other fragment anions (except NH₂⁻ formation, see discussion below).

Although (Pu-H)⁻ (FIG. 6b)) is the dominant fragment anion from purine at K collision energies below 16 eV, it only accounts for (70 \pm 7)% of the total anion yields at 5.8 eV and falls to just (35 \pm 7)% at 3.8 eV available energy. At this low collision energy (12 eV in the lab frame), (Pu-H)⁻ and NH⁻ are the prevalent yields, with the latter contributing to 20% of the fragmentation pattern. By analogy with adenine where the threshold for H abstraction from N9 in DEA experiments is 0.94 eV,¹⁴ we expect that any fragment anion has to be formed after H abstraction from purine TNI. We also observe strong competition with CN⁻ formation which is visible at lab frame collision energies above 30 eV for both adenine and purine.

From TABLE I we observe loss of more than one hydrogen atom from Pu, Ad, 9-mAd and 6-dimAd. In the case of 2-DAd we have detected (2-DAd-H)⁻ only at 100 eV lab frame collision energy. Huber *et al.*'s⁶ DEA experiments on adenine have reported the loss of two H atoms

through reactions yielding $(M-2H)^- + H_2$ and/or $(M-2H)^- + 2H$ formation. Loss of H_2 was attributed to the 0.7 eV resonance whereas $H + H$ formation was accessible from the two high energy resonances at 7 and 10.6 eV, and loss of an $H_2 + H$ (or three H atoms) was reported at 6.5 and 10.9 eV resonances.⁶ As these fragment anions are discernible in the present mass spectra above a lab frame collision energy of 30 eV (16.6 eV available energy), we conclude that these reactions are also accessible in potassium-adenine collisions. The lack of $(M-D)^-$ signal from 2-DAd was proposed in terms of strong autodetachment competing with dissociation as well as to the lack of electron spin density in the C2 position. For more details see Ref. ¹¹ Finally, the underlying molecular mechanisms yielding $(M-2H)^-$ and $(M-3H)^-$ formation are still not yet clear, although we suggest H_2 or $2H$ formation (depending on the specific anionic states involved) and the loss of H_2 plus an H radical or $H+H+H$, respectively, as proposed by Huber and co-workers.⁶ In the case of 2-DAd, however, $(M-HD)^-$ formation is absent which can be related to the lack of electrostatic potentials around C2 as well as to enhanced autodetachment due to isotopic labelling. Further investigations are needed to clarify these processes, notably with isotopic labelling in other positions.

B. $(M-CH_3)^-$ and $(M-NH_2)^-$

Formation of $(M-CH_3)^-$ and $(M-NH_2)^-$ from potassium collisions with 9-methyl adenine occurs at 67 eV in the centre-of-mass frame (see FIG.5). The electron spin densities in FIG. 2 for 9-methyl adenine suggest that the electron may be initially transferred to the π_2^* and π_3^* states and subsequently to the σ_1^* state, resulting in dissociation. Alternatively, a direct initial transfer to the σ_1^* state and subsequent dissociation may occur. The present work does not provide evidence to assess the relative contributions of these two plausible pathways. It is interesting to note that similar dynamics have been discussed by Almeida *et al.*⁴⁰ in pyrimidine bases. In the case of 3-methyl uracil, the closeness of the vertical transition energies of the π^* and σ^* states did not allow us to specify the dominant pathway to dissociation.

The loss of a CH_3 group is only visible from 9-mAd and 6-dimAd (respectively yielding ions with m/z 134 and 148 – see Fig. 3 and Fig. 5) but there is no evidence for these channels at 15 eV lab frame¹¹. This suppression can be rationalised in terms of a slow collision process (~ 68 fs) enhancing Coulomb stabilization of the TNI by the proximate K^+ ion, increasing the probability of intramolecular electron transfer that may favour dissociation (as is the case for NH_2^- formation, see Section IV.F) or may favour autodetachment (suppressing dissociation). As far as authors are aware, no DEA experiments have been produced these fragment anions.

Now we turn to the loss of an NH₂ group from adenine (TABLE I) producing a negative ion with m/z 119 (see also FIG. 3). The DEA data of Huber *et al.*⁶ reveals a dissociation channel at low electron energies, with a notably strong resonance feature at 0 eV indicating an exothermal character to the decomposition reaction. The TOF mass spectrum at 12 eV (not shown here) and 15 eV lab frame collision energy¹¹ show no traces of (Ad-NH₂)⁻ formation. This can be explained under the same rationale of longer transit time of K⁺ near the TNI promoting either autodetachment or an alternative dissociation, which are reasonable arguments given the prominent decrease of (Ad-H)⁻ BR at these energies as well as other fragment anions formation (see FIG. 6a).

C. Loss of HCN

Hydrogen cyanide abstraction is more evident in the TOF mass spectra of Pu, Ad and 9-mAd (FIG. 5) leading to ring opening, with assignment of the fragment anions indicated in TABLE I, where arrows indicate the sequential HCN abstractions. The HOMOs of Ad and 9-mAd in FIG. 1 are localized on the rings showing relevant π character while the LUMOs appear with strong π^* antibonding with nodes along the C–N bonds. Such electron spin densities are indicative of favourable bond breaking in particular where curve crossing in the diabatically frame description may be relevant (i.e. π_4^*/σ_2^*). Though such cleavage, e.g. C2-N1, C4-N3 and C5-N7, C8-N9, may leave the remaining neutral HCN intact.

Within the collision energy range studied for adenine and its derivatives, i.e. for the available energy (3.8–68.3 eV), such loss of HCN units is operative since the estimated threshold of the decomposition reaction requires 3.89 eV given that $\Delta_f H_g^\circ$ (C₅H₅N₅) = 225.7 kJ/mol (2.34 eV),⁴¹ $\Delta_f H_g^\circ$ (C₄H₃N₄)⁻ = 248 kJ/mol (2.57 eV),⁴² $\Delta_f H_g^\circ$ (HCN) = 135.14 kJ/mol (1.4 eV)⁴² and $\Delta_f H_g^\circ$ (H) = 218 kJ/mol (2.26 eV).⁴² It is interesting that the loss of HCN from 9-mAd follows methyl abstraction from the TNI, whereas in Pu and Ad it takes place after dehydrogenation of the parent anion. In the case of adenine, Huber *et al.*⁶ reported that fragment anion 107 u, (C₄H₃N₄)⁻, is formed through loss of HCN from the dehydrogenated parent anion since this reaction is energetically more favourable than CN radical and H₂ formation.

D. C₃N⁻

The formation of fragment anion with m/z 50 from Ad, 9-mAd and 2-DAd (FIG. 5) is just visible at 100 eV lab frame collision energy and totally suppressed at 15 eV.¹¹ Harrison and Tennyson⁴³ have recently reported that C₃N⁻ supports a number of low-lying dissociative TNI states. The BR of C₃N⁻ in FIG. 6a) shows the threshold of formation at ~ 31 eV available energy

and increases as a function of the collision energy. We also observe that above this energy the cyanide anion is present in the BRs. Although C_3N has higher electron affinity (4.54 eV⁴⁴) than CN (3.862 eV⁴⁵), the former anion results from combined fragmentation of both of rings with a considerable energy requirement. Owing to the molecular structure of Ad, C_3N^- can only result from the pyrimidine-like structure decomposition whereas CN^- formation may proceed from the breaking of the five-membered ring in particular in the lower energy regime (see discussion below). Interesting to note that we have previously observed C_3N^- fragments from potassium collisions with thymine.⁴⁶ We suggest that in the case of adenine, this fragment anion may be formed via concerted mechanisms involving the six-membered ring.

E. CN^-

The TOF mass spectra in FIG. 5 at 100 eV lab frame collision energy are dominated by the cyanide anion whereas at low collision energies only $(M-H)^-$, H^- , NH^- , and NH_2^- are discernible.¹¹ Hence we can conclude that in the unimolecular decomposition process, the dehydrogenated parent anion is a precursor in the formation of fragments that require bond cleavages in the rings, namely CN^- . Such a decomposition process was previously observed for the pyrimidines investigated in collisional electron transfer experiments.⁴⁷ DEA experiments on adenine show that CN^- is the most intense anion at electron energies above 5 eV, with resonances at 5.8, 6.7 and 11.5 eV.⁶ In order to aid our understanding of the underlying molecular mechanisms and the accessed states that are responsible for CN^- formation in adenine-potassium collisions, FIG. 2 shows three calculated π^* orbitals at 4.3 eV (π_1^*), 5.5 eV (π_2^*) and 7.0 eV (π_3^*). At higher energies two σ^* resonances at 8.8 (σ_3^*) and 10.3 eV (σ_4^*) are present, with σ_3^* along the C2–N1 bond. Note that there is no appreciable difference as to the energy of 9-mAd LUMOs. Accordingly, the adenine BRs in FIG. 6a) show that CN^- cannot be produced ≤ 6.1 eV (≤ 15 eV collision energy) which can be related to an electron promotion to the π_2^*/π_3^* orbital. Accessing π_3^* is achieved by increasing the collision energy, and so the CN^- yield, with bond-breaking certainly occurring through access of the σ^* states. Now, a question that stands to be answered is where does CN^- formation proceed from? At threshold, is it initially formed from the fragmentation of the five-membered ring or is it the result of a combined contribution of breaking both rings? A careful inspection of FIG. 5 (100 eV lab-frame collision energy) for Ad and 9-mAd shows a weak fragment anion at 107 u that has been assigned in TABLE I to $(C_4H_3N_4)^-$ but is totally suppressed at 15 eV lab frame collision energy.¹¹ The BRs in Fig. 6 indicate that fragment anions (with the exception of NH_2^-) result from decomposition of the dehydrogenated parent anion, and this rationale also holds for 9-

mAd. By analogy with Denifl *et al.*'s¹⁴ DEA experiments, this signifies that H abstraction is already operative at ~ 1 eV. In the case of potassium-adenine collisions, the dehydrogenated parent anion may be formed with an excess of internal energy resulting in fragmentation yielding two complementary channels:



These fragmentation pathways may proceed through two routes which involve breaking of N1-C6 and C6-C5 bonds (six-membered ring), and N7-C8 and N9-C4 bonds (five-membered ring). $(\text{C}_4\text{H}_3\text{N}_4)^-$ formation may proceed from both routes at high collision energies (typically 100 eV in the lab frame). Breaking N7-C8 and N9-C4 bonds is the most probable route at low collision energies, corresponding to the calculated π_2^* and π_3^* molecular orbitals, and most likely leading to the formation of CN^- in view of its high electron affinity (3.8620 ± 0.0050 eV).⁴²

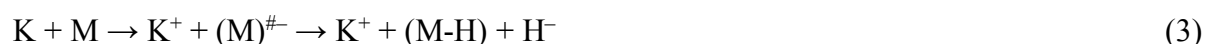
F. NH_2^- and NH^-

The TOF mass spectrum of Pu at 15 eV lab frame collision energy¹¹ shows a significant contribution of NH^- and NH_2^- relative to the $(\text{Pu-H})^-$ yield. In the case of Ad at 12 eV (see its BR in FIG. 6a) we observe that $\text{NH}_2^-/(\text{Ad-H})^-$ appears at a ratio of $\sim 1:2$. The NH_2^- threshold of formation from adenine in DEA was estimated at ~ 3.1 eV given that $D(\text{C-NH}_2) = 3.9$ eV⁵ and $\text{EA}(\text{NH}_2) = (0.771 \pm 0.005)$ eV.⁴⁸ The BRs in Fig. 6 show that NH_2^- is not formed by dissociation of the dehydrogenated parent anion. At 12 eV lab frame collision energy, the available energy amounts to 4.0 eV which is enough to yield the NH_2 anion. At 6.1 eV available energy (15 eV in the lab frame), the TNI is formed with an excess of internal energy which can be statistically distributed over the internal degrees of freedom, resulting in NH_2^- formation even with a modest electron affinity. This assumption seems reasonable since the electrostatic potential maps of Ad show a region of positive electron spin density around the $-\text{NH}_2$ group.¹⁴ However, the high relative intensity of the NH_2^- signal in the present data at low collision energies can only be attributed to the presence of K^+ in the vicinity of the TNI allowing intramolecular electron transfer from the ring to $-\text{NH}_2$. In the case of Pu, NH^- and NH_2^- formation mechanism may substantially differ from Ad. The isodensity map of purine in Ref. 14 shows that the region strongly favourable for electron capture is around the N9-H and the neighbouring C8-H sites. As such, NH^- formation upon electron transfer to purine may proceed through the breaking of C4-N9 and C8-N9 bonds and electron capture at NH. Taking $D(\text{C-N}) = 3.1$ eV and $\text{EA}(\text{NH})$

= (0.370 ± 0.004) eV,⁴² the estimated threshold is 5.83 eV. The available energy at a lab-frame collision energy of 15 eV is slightly higher than this value and hence this formation mechanism is plausible in the present experiments. Finally, regarding NH_2^- formation from purine, we note from FIG. 6b) that its yield is slightly lower than NH^- formation. The $\text{NH}_2^- / \text{NH}^-$ ratio remains approximately constant when the collision energy is increased to 30 eV lab frame (16 eV available energy, FIG. 6b), indicating that the two fragments derive from a common excited precursor. The mechanism for amino radical anion formation must involve NH combining with a proton transferred from the C8 position. Identifying the specific mechanism is beyond the scope of this contribution and quantum chemical calculations would be very helpful clarifying the routes of NH_2^- formation.

G. H^-

The formation of H^- can be represented by the reaction:



The H^- yield is clearly visible in 30 eV lab frame collisions (FIG. 3) from Pu only. We do not have a strong basis to explain the absence (with the present signal/noise ratios) of this anion in the equivalent mass spectra of Ad and 6-dimAd. Huber *et al.*⁶ have reported H^- formation via two resonances at 6 and 11 eV, the former almost three times more intense than the latter. The resonance at 6 eV may be accessed in potassium collision at 15 eV lab frame (~ 6 eV available energy). We observe H^- formation from adenine in 100 eV lab frame collisions (FIG. 5), albeit with a very low yield. This may suggest that its absence in the present measurements at low collision energies is linked to strong competition with other fragment anion channels with energetically-similar resonances.

V. CONCLUSIONS

The present work provides a comprehensive investigation of the decomposition mechanisms of Pu, Ad, 9-mAd, 6-dimAD and 2-DAd in collisions with potassium atoms. The major fragment anions formation have been investigated as a function of the available energy in the centre-of-mass frame. In the case of adenine, the dehydrogenated parent anion is shown to be a precursor in the formation of the smaller fragment anions, with the exception of NH_2^- . We report for the first time formation of $(\text{M-CH}_3)^-$ from 9-mAd and 6-dimAd. Additionally, C_3N^- formation is proposed to proceed through the six-membered ring structure decomposition while the cyanide

anion may proceed from the breaking of the five-membered ring particularly in low energy collisions. The theoretical calculations reveal how the electronic structures of Ad and 9-mAd are modified by the presence of the electron donor and hence provide insights into the electronic states that are most likely participate in the major fragment anion channels. The clear differences in fragment anion production from adenine in the present electron transfer collisions compared with DEA provide further evidence that the specifics of the electron delivery mechanisms need to be properly taken into account in nanoscale models of radiation damage to DNA.

ACKNOWLEDGMENTS

TC, MM and FFS acknowledge the Portuguese National Funding Agency FCT-MCTES through SFRH/BD/52538/2014, PD/BD/106038/2015 and researcher position IF-FCT IF/00380/2014, respectively, and together with PLV the research grant UID/FIS/00068/2013. This work was also supported by Radiation Biology and Biophysics Doctoral Training Programme (RaBBiT, PD/00193/2010); UID/Multi/ 04378/2013 (UCIBIO). GG acknowledges partial financial support from the Spanish Ministerio de Economía, Industria y Competitividad (Project No. FIS2016-80440). SE acknowledges the support of the British EPSRC through a Career Acceleration Fellowship (EP/J002577/1) and a Research Grant (EP/L002191/1). MCB acknowledges support from the computational resources from the CCIN2P3 in Villeurbanne and CCRT/CINES/IDRIS by GENCI (Grand Equipement National de Calcul Intensif) under the allocation x2017087662.

REFERENCES

- ¹ B. Boudaiffa, P. Cloutier, D. Hunting, M.A. Huels, and L. Sanche, *Science* **287**, 1658 (2000).
- ² I. Baccarelli, I. Bald, F.A. Gianturco, E. Illenberger, and J. Kopyra, *Phys. Rep.* **508**, 1 (2011).
- ³ L. Sanche, *Nature* **461**, 358 (2009).
- ⁴ C.R. Wang, J. Nguyen, and Q. Bin Lu, *J. Am. Chem. Soc.* **131**, 11320 (2009).
- ⁵ H. Abdoul-Carime, J. Langer, M.A. Huels, and E. Illenberger, *Eur. Phys. J. D* **35**, 399 (2005).
- ⁶ D. Huber, M. Beikircher, S. Denifl, F. Zappa, S. Matejcik, A. Bacher, V. Grill, T.D. Märk, and P. Scheier, *J. Chem. Phys.* **125**, 84304 (2006).
- ⁷ B.F. Minaev, M.I. Shafranyosh, Y. Svida, M.I. Sukhoviya, I.I. Shafranyosh, G. V. Baryshnikov, and V.A. Minaeva, *J. Chem. Phys.* **140**, 175101 (2014).
- ⁸ C. Desfrancois, H. Abdoul-Carime, and J.P. Schermann, *J. Chem. Phys.* **104**, 7792 (1996).
- ⁹ K. Aflatooni, G.A. Gallup, and P.D. Burrow, *J. Phys. Chem. A* **102**, 6205 (1998).
- ¹⁰ K. Aflatooni, A.M. Scheer, and P.D. Burrow, *J. Chem. Phys.* **125**, 1 (2006).
- ¹¹ T. Cunha, M. Mendes, F. Ferreira da Silva, S. Eden, G. Garcia, and P. Limão-Vieira, *J. Chem. Phys.* **148**, (2018).
- ¹² H. Abdoul-Carime, S. Gohlke, and E. Illenberger, *Phys. Rev. Lett.* **92**, 168103 (2004).
- ¹³ S. Gohlke, H. Abdoul-Carime, and E. Illenberger, *Chem. Phys. Lett.* **380**, 595 (2003).
- ¹⁴ S. Denifl, P. Sulzer, D. Huber, F. Zappa, M. Probst, T.D. Märk, P. Scheier, N. Injan, J. Limtrakul, R. Abouaf, and H. Dunet, *Angew. Chem. Int. Ed.* **46**, 5238 (2007).
- ¹⁵ S. Tonzani and C.H. Greene, *J. Chem. Phys.* **124**, 54312 (2006).
- ¹⁶ M. Harańczyk, M. Gutowski, X. Li, and K.H. Bowen, *Proc Natl Acad Sci USA* **104**, 4804 (2007).
- ¹⁷ C. Fonseca Guerra, F.M. Bickelhaupt, S. Sana, and F. Wang, *J. Phys. Chem. A* **110**, 4012 (2006).
- ¹⁸ L.M. Salter and G.M. Chaban, *J. Phys. Chem. A* **106**, 4251 (2002).
- ¹⁹ M.P. Fulscher, L. Serrano-Andres, and B.O. Roos, *J. Am. Chem. Soc.* **119**, 6168 (1997).
- ²⁰ A.C. Borin, L. Serrano-Andres, M.P. Fulscher, and B.O. Roos, *J. Phys. Chem. A* **103**, 1838 (1999).
- ²¹ S. Pilling, A.F. Lago, L.H. Coutinho, R.B. de Castilho, G.G.B. de Souza, and A.N. de Brito, *Rapid Commun. Mass Spectrom.* **21**, 3646 (2007).
- ²² B. Barc, M. Ryszka, J.C. Pouilly, E. Jabbour Al Maalouf, Z. El Otell, J. Tabet, R. Parajuli, P.J.M. Van Der Burgt, P. Limão-Vieira, P. Cahillane, M. Dampc, N.J. Mason, and S. Eden, *Int. J. Mass Spectrom.* **365–366**, 194 (2014).
- ²³ S. Chakrabarti and S.K. Chakrabarti, *Astron. Astrophys.* **8**, 9 (2000).

- ²⁴ R. Glaser, B. Hodgen, D. Farrelly, and E. McKee, *Astrobiology* **7**, 455 (2007).
- ²⁵ V.P. Gupta, P. Tandon, P. Rawat, R.N. Singh, and A. Singh, *A&A* **528**, A129 (2011).
- ²⁶ D. Almeida, F. Ferreira da Silva, G. García, and P. Limão-Vieira, *Phys. Rev. Lett.* **110**, 1 (2013).
- ²⁷ F. Ferreira da Silva, D. Almeida, R. Antunes, G. Martins, Y. Nunes, S. Eden, G. Garcia, and P. Limão-Vieira, *Phys. Chem. Chem. Phys.* **13**, 21621 (2011).
- ²⁸ R. Antunes, D. Almeida, G. Martins, N.J. Mason, G. Garcia, M.J.P. Maneira, Y. Nunes, and P. Limão-Vieira, *Phys. Chem. Chem. Phys.* **12**, 12513 (2010).
- ²⁹ D. Almeida, M.-C. Bacchus-Montabonel, F. Ferreira da Silva, G. Garcia, and P. Limão-Vieira, *J. Phys. Chem. A* **118**, 6547 (2014).
- ³⁰ M.C. Bacchus-Montabonel and Y.S. Tergiman, *Comput. Theor. Chem* **990**, 177 (2012).
- ³¹ M.C. Bacchus-Montabonel and F. Calvo, *Phys. Chem. Chem. Phys.* **17**, 9629 (2015).
- ³² L. Salem, *Electrons in Chemical Reactions: First Principles* (Wiley Interscience: New York, 1982).
- ³³ M.C. Bacchus-Montabonel, D. Talbi, and M. Persico, *J. Phys. B: At. Mol. Opt. Phys.* **33**, 955 (2000).
- ³⁴ M. Fuentes-cabrera, B.G. Sumpter, and J.C. Wells, *J Phys Chem B* **109**, 21135 (2005).
- ³⁵ M.C. Bacchus-Montabonel and Y.S. Tergiman, *Phys. Rev. A* **74**, 54702 (2006).
- ³⁶ M.C. Bacchus-Montabonel and Y.S. Tergiman, *Phys. Chem. Chem. Phys.* **13**, 9761 (2011).
- ³⁷ H.-J. Werner, P.J. Knowles, F.R. Manby, M. Schütz, P. Celani, G. Knizia, T. Korona, R. Lindh, A. Mitrushenkov, and G. Rauhut, (2012).
- ³⁸ A. Nicklass, M. Dolg, H. Stoll, and H. Preuss, *J. Chem. Phys.* **102**, 8942 (1995).
- ³⁹ Y. Kanazawa, M. Ehara, and T. Sommerfeld, *J. Phys. Chem. A* **120**, 1545 (2016).
- ⁴⁰ D. Almeida, D. Kinzel, F. Ferreira da Silva, B. Puschnigg, D. Gschliesser, P. Scheier, S. Denifl, G. García, L. González, and P. Limão-Vieira, *Phys. Chem. Chem. Phys.* **15**, 11431 (2013).
- ⁴¹ O. V. Dorofeeva and N. Vogt, *J. Chem. Eng. Data* **54**, 1348 (2009).
- ⁴²<http://webbook.nist.gov/chemistry/> (2018).
- ⁴³ S. Harrison and J. Tennyson, *J. Phys. B: At. Mol. Opt. Phys.* **44**, 45206 (2011).
- ⁴⁴ K. Graupner, T.L. Merrigan, T.A. Field, T.G.A. Youngs, and P.C. Marr, *New J. Phys* **8**, 117 (2006).
- ⁴⁵ S.E. Bradforth, E.H. Kim, D.W. Arnold, and D.M. Neumark, *J. Chem. Phys.* **98**, 800 (1993).
- ⁴⁶ D. Almeida, R. Antunes, G. Martins, S. Eden, F. Ferreira da Silva, Y. Nunes, G. Garcia, and P. Limão-Vieira, *Phys. Chem. Chem. Phys.* **13**, 15657 (2011).

⁴⁷ F. Ferreira da Silva, C. Matias, D. Almeida, G. García, O. Ingólfsson, H.D. Flosadóttir, B. Ómarsson, S. Ptasinska, B. Puschnigg, P. Scheier, P. Limão-Vieira, and S. Denifl, *J. Am. Soc. Mass Spectrom.* **24**, 1787 (2013).

⁴⁸ C.T. Wickham-Jones, K.M. Ervin, G.B. Ellison, and W.C. Lineberger, *J. Chem. Phys.* **91**, 2762 (1989).

Figure captions

FIG. 1. Molecular structure of adenine and 9-methyl adenine.

FIG. 2. Calculated highest occupied molecular orbitals (HOMOs) and lowest unoccupied molecular orbitals (LUMOs) for 9-methyl adenine (9-mAd) and adenine (Ad) in the presence of a potassium cation atom in the perpendicular geometry pointing on the N9 atom. In parenthesis values calculated without the presence of potassium. Energies in eV.

FIG. 3. Time-of-flight negative ion mass spectra in potassium-purine (Pu), -adenine (Ad) and -6-dimethyl adenine (6-dimAd) collisions at 30 eV lab frame energy (16.0, 16.6 and 17.4 eV available energy in the centre-of-mass, respectively). See text for details.

FIG. 4. Time-of-flight negative ion mass spectra in potassium-adenine (Ad) and - purine (Pu) collisions at 70 eV lab frame energy (44.5 and 43.2 eV available energy in the centre-of-mass, respectively). See text for details and note that an alternative view of these results is presented in our recent communication about formation of dehydrogenated parent anions ((M-H)⁻) [Ref 11].

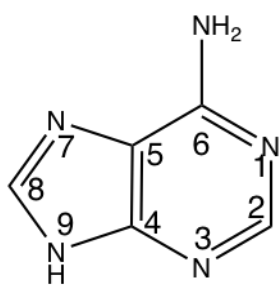
FIG. 5. Time-of-flight negative ion mass spectra in potassium-purine (Pu), -adenine (Ad), -adenine-2-d (2-DAd), -9-methyl adenine (9-mAd) and collisions at 100 eV lab frame collision energy (63.6, 65.5, 65.6 and 67.0 eV available energy in the centre-of-mass frame, respectively). See text for details.

FIG. 6. Branching ratios (fragment anion yield/total anion yield) as a function of the collision energy in the centre-of-mass frame: a) adenine (Ad); b) purine (Pu). See text for details.

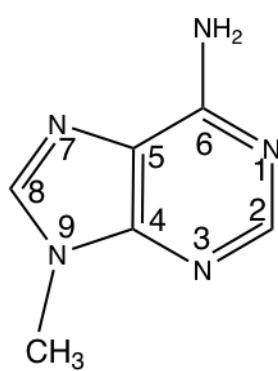
Table caption

TABLE I. Negative ions formed in potassium collisions with purine (Pu), adenine (Ad), 9-methyl adenine (9-mAd), 6-dimethyl adenine (6-dimAd) and adenine-2-d (2-DAd). Arrows indicate loss of HCN.

FIG. 1. Molecular structure of adenine and 9-methyl adenine.



adenine



9-methyl adenine

FIG. 2. Calculated highest occupied molecular orbitals (HOMOs) and lowest unoccupied molecular orbitals (LUMOs) for 9-methyl adenine (9-mAd) and adenine (Ad) in the presence of a potassium cation atom in the perpendicular geometry pointing on the N9 atom. In parenthesis values calculated without the presence of potassium. Energies in eV.

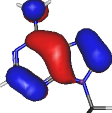
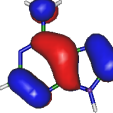
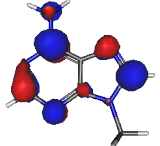

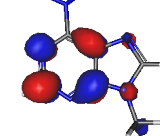
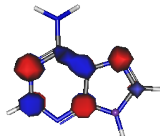
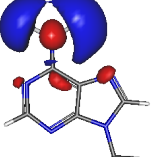
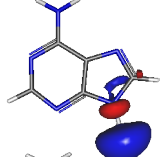
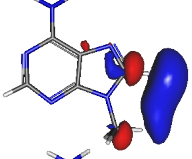
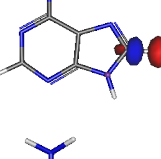
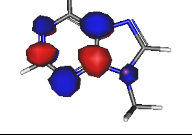
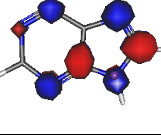
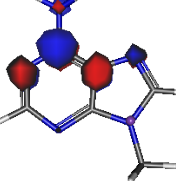
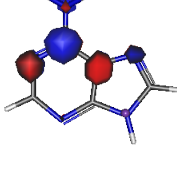
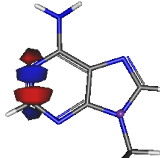
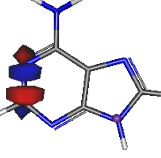
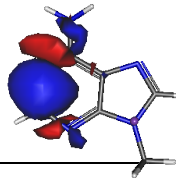
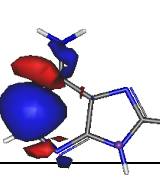
9-methyl adenine (9-mAd)	adenine (Ad)
HOMO 	HOMO 
π_1^* 4.4 eV (2.6 eV) 	π_1^* 4.3 eV (2.6 eV) 
π_2^* 5.5 eV (3.5 eV) 	π_2^* 5.5 eV (3.4 eV) 
σ_1^* 6.0 eV (5.8 eV) 	σ_1^* 5.8 eV (5.6 eV) 
σ_2^* 6.2 eV 	σ_2^* 6.2 eV 
π_3^* 7.2 eV (4.6 eV) 	π_3^* 7.0 eV (4.6 eV) 
π_4^* 8.4 eV 	π_4^* 8.2 eV 
σ_3^* 8.8 eV 	σ_3^* 8.8 eV 
σ_4^* 10.4 eV 	σ_4^* 10.3 eV 

FIG. 3. Time-of-flight negative ion mass spectra in potassium-purine (Pu), -adenine (Ad) and -6-dimethyl adenine (6-dimAd) collisions at 30 eV lab frame energy (16.0, 16.6 and 17.4 eV available energy in the centre-of-mass, respectively). See text for details.

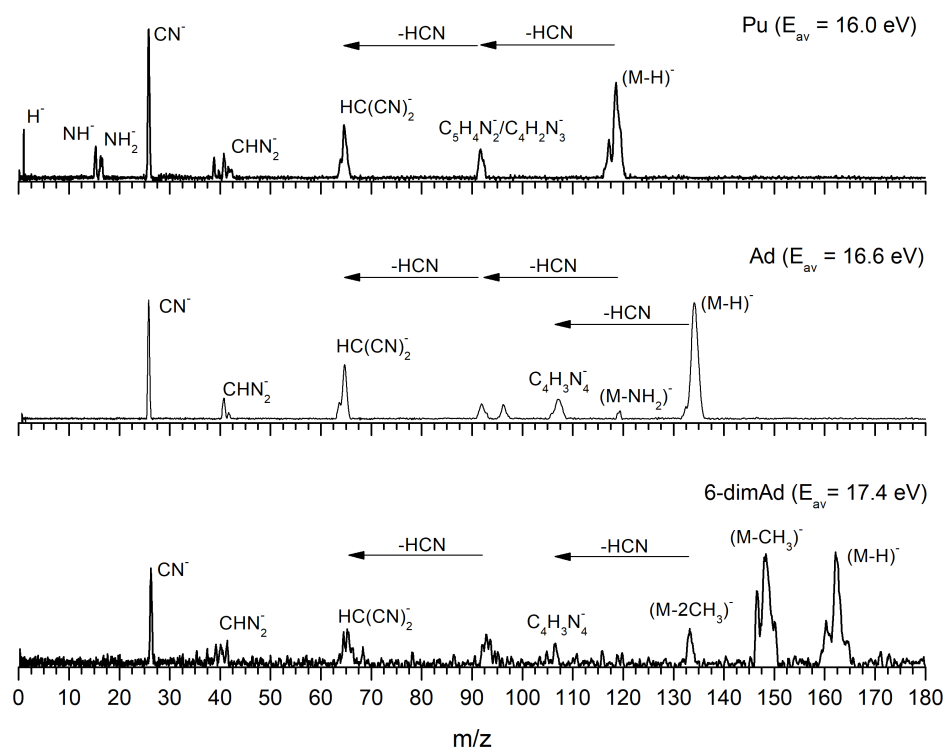


FIG. 4. Time-of-flight negative ion mass spectra in potassium-adenine (Ad) and - purine (Pu) collisions at 70 eV lab frame energy (44.5 and 43.2 eV available energy in the centre-of-mass, respectively). See text for details.

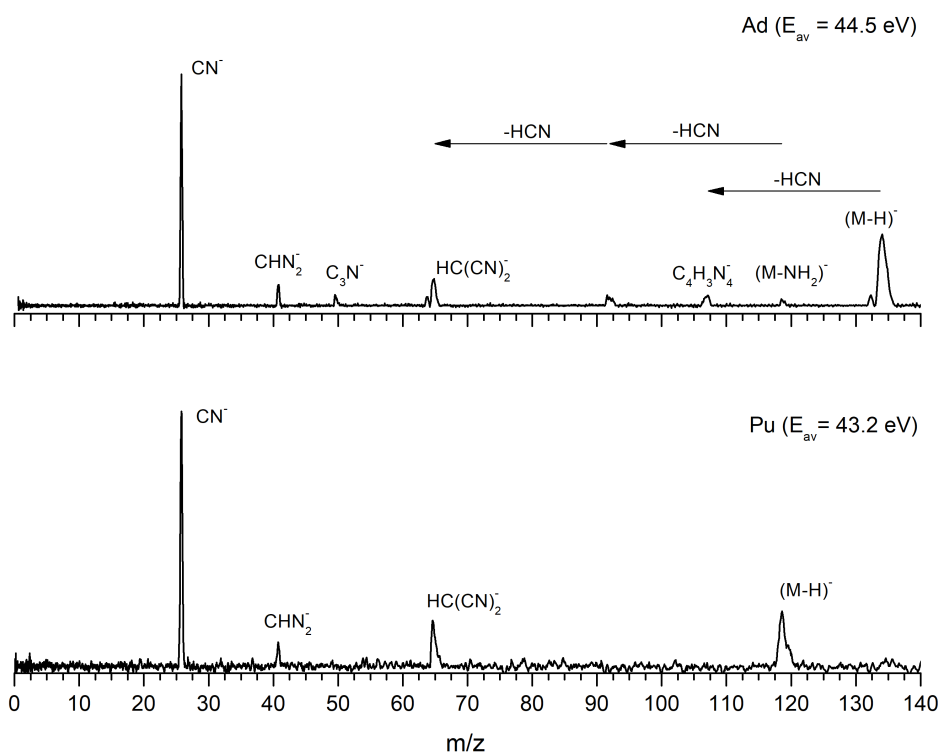


FIG. 5. Time-of-flight negative ion mass spectra in potassium-purine (Pu), -adenine (Ad), -adenine-2-d (2-DAd), -9-methyl adenine (9-mAd) and collisions at 100 eV lab frame collision energy (63.6, 65.5, 65.6 and 67.0 eV available energy in the centre-of-mass frame, respectively). See text for details and note that an alternative view of these results is presented in our recent communication about formation of dehydrogenated parent anions ((M-H)⁻) [Ref 11].

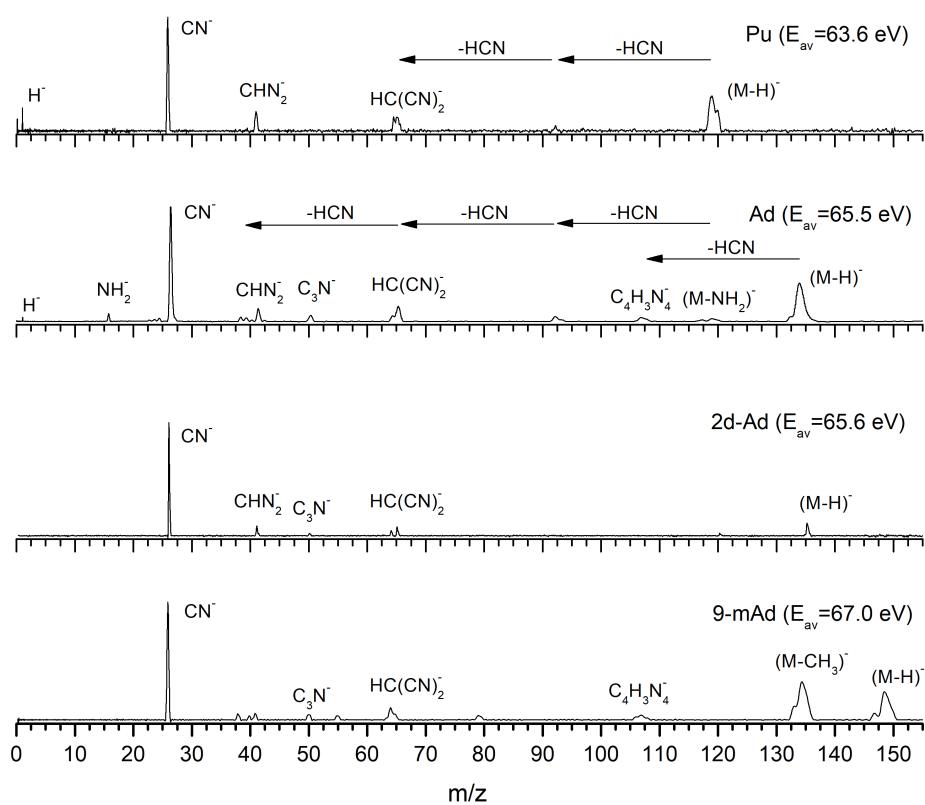
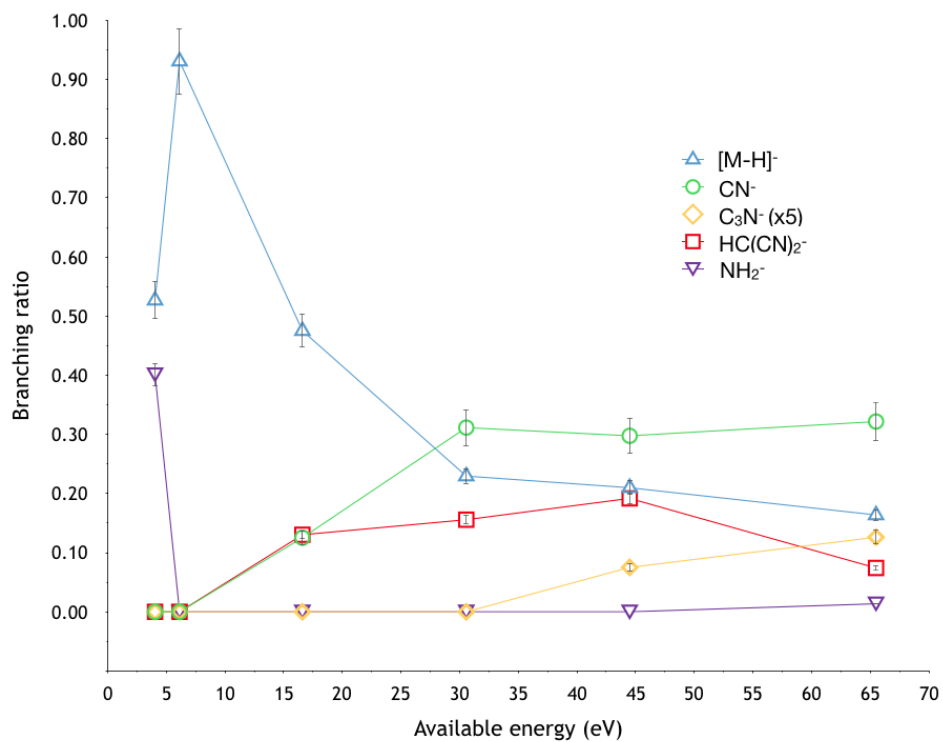


FIG. 6. Branching ratios (fragment anion yield/total anion yield) as a function of the collision energy in the centre-of-mass frame: a) adenine (Ad); b) purine (Pu). See text for details.

a) adenine (Ad)



b) purine (Pu)

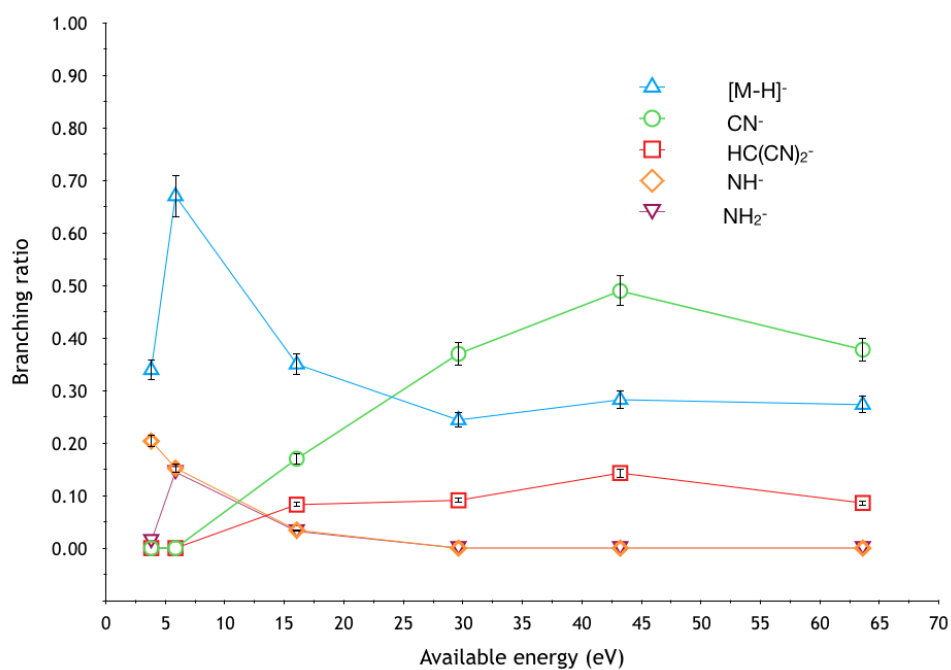


TABLE I. Negative ions formed in potassium collisions with purine (Pu), adenine (Ad), 9-methyl adenine (9-mAd), 6-dimethyl adenine (6-dimAd) and adenine-2-d (2-DAd). Arrows indicate loss of HCN.

Mass (u)	Pu	Ad	9-mAd	6-dimAd	2-DAd
1	H ⁻	H ⁻	H ⁻		
15	NH ⁻				
16	NH ₂ ⁻	NH ₂ ⁻	NH ₂ ⁻		
26	CN ⁻	CN ⁻	CN ⁻	CN ⁻	CN ⁻
38		C ₂ N ⁻	C ₂ N ⁻		
40			CN ₂ ⁻ /C ₂ H ₂ N ⁻		
41	CHN ₂ ⁻ /C ₂ H ₃ N ⁻	CHN ₂ ⁻ /C ₂ H ₃ N ⁻	CHN ₂ ⁻ /C ₂ H ₃ N ⁻	CHN ₂ ⁻ /C ₂ H ₃ N ⁻	CHN ₂ ⁻ /C ₂ H ₃ N ⁻
42	CH ₂ N ₂ ⁻ /C ₂ H ₄ N ⁻	CH ₂ N ₂ ⁻ /C ₂ H ₄ N ⁻			
50		C ₃ N ⁻	C ₃ N ⁻		C ₃ N ⁻
55			C ₃ H ₅ N ⁻		
64	C ₃ N ₂ ⁻	C ₃ N ₂ ⁻	C ₃ N ₂ ⁻		C ₃ N ₂ ⁻
65	((CN) ₂ HC) ⁻	((CN) ₂ HC) ⁻		((CN) ₂ HC) ⁻	((CN) ₂ HC) ⁻
79			C ₄ H ₃ N ₂ ⁻		
80			C ₄ H ₃ N ₂ ⁻		
92	(Pu-H-HCN) ⁻	C ₅ H ₄ N ₂ ⁻		C ₅ H ₄ N ₂ ⁻	
96		C ₃ H ₄ N ₄ ⁻			
107		C ₄ H ₃ N ₄ ⁻	C ₄ H ₃ N ₄ ⁻		
108		C ₄ H ₄ N ₄ ⁻			
117		(Ad-H(NH ₃)) ⁻			
118	(Pu-2H) ⁻				
119	(Pu-H) ⁻	(Ad-NH ₂) ⁻			
120					(2-DAd-NH ₂) ⁻
132		(Ad-3H) ⁻			
133		(Ad-2H) ⁻	(9-mAd-HCH ₃) ⁻	(6-dimAd-(CH ₃) ₂) ⁻	
134		(Ad-H) ⁻	(9-mAd-CH ₃) ⁻		
135					(2-DAd-H) ⁻
146				(6-dimAd-NH ₃) ⁻	
147			(9-mAd-2H) ⁻		
148			(9-mAd-H) ⁻	(6-dimAd-CH ₃) ⁻	
160				(6-dimAd-3H) ⁻	
162				(6-dimAd-H) ⁻	